Ultrafast adsorption of heavy metal ions onto functionalized lignin-based hybrid magnetic nanoparticles

Zhang, Weihua; Shuzhen, Ni; Wang, Xiaoju; Zhang, Yongchao; Lagerquist, Lucas; Qin, Menghua; Willför, Stefan; Xu, Chunlin; Fatehi, Pedram

Published in:
Chemical Engineering Journal

DOI:
10.1016/j.cej.2019.04.111

Published: 01/01/2019

Document Version
Submitted manuscript

Document License
Publisher rights policy

Ultrafast adsorption of heavy metal ions onto functionalized lignin-based hybrid magnetic nanoparticles

Yongchao Zhang [a,b], Shuzhen Ni [e], Xiaoju Wang [a], Weihua Zhang [a], Lucas Lagerquist [c], Menghua Qin [d], Stefan Willför [a], Chunlin Xu [a]*, Pedram Fatehi [b]*

[a] Johan Gadolin Process Chemistry Centre, c/o Laboratory of Wood and Paper Chemistry, Åbo Akademi University, Turku FI-20500, Finland

[b] Department of Chemical Engineering, Lakehead University, Thunder Bay, Ontario P7B 5E1, Canada

[c] Johan Gadolin Process Chemistry Centre, c/o Laboratory of Organic Chemistry, Åbo Akademi University, Turku Fi-20500, Finland

[d] Organic Chemistry Laboratory, Taishan University, Taian 271021, Shandong, China

[e] Jiangsu Co-Innovation Center for Efficient Processing and Utilization of Forest Resources, Nanjing Forestry University, Nanjing 210037, Jiangsu, China

Corresponding authors

* Johan Gadolin Process Chemistry Centre, c/o Laboratory of Wood and Paper Chemistry, Åbo Akademi University, Turku FI-20500, Finland. E-mail: cxu@bo.fi; Tel: +358408362088

* Department of Chemical Engineering, Lakehead University, Thunder Bay, ON P7B 5E1, Canada. E-mail: pfatehi@lakeheadu.ca; Fax: +807-346-7943; Tel: +807-343-8697

Abstract:

Heavy metals have raised an increasing number of pollution incidents and resulted in potent damages to aquatic ecosystems and human health. Thus, effective and efficient approaches to eliminate heavy metal ions are in urgent needs. Herein, novel hybrid nanoparticles have been prepared by a facile method using epichlorohydrin as a cross-linker between amino-functionalized magnetic nanoparticles and carboxymethylated lignin. Multiple characterization methods including XRD, FTIR, XPS, SEM, and TEM confirmed the formed nanostructures and the chemical features of the lignin-based hybrid nanoparticles. The as-synthesized hybrid nanoparticles exhibited high adsorption capacities of 150.33 and 70.69 mg/g for Pb^{2+} and Cu^{2+}, respectively. More importantly, the adsorption equilibriums of Pb^{2+} and Cu^{2+} onto hybrid nanoparticles can be achieved within 30 seconds, which are among the fastest functional adsorbents for Pb^{2+} and Cu^{2+} removal as reported by now. The ultrafast adsorption is ascribed not only to the nanostructures, but also to the abundant active sites provided by the carboxymethylated lignin. The mechanism of removing Pb^{2+} and Cu^{2+} by hybrid nanoparticles could be mainly attributed to ion exchange and hydrogen bonding. The tailored nanostructured hybrid nanoparticles with exceptional adsorption effectiveness and efficiency are low-cost and eco-friendly, which potentially meets the cost-effective criteria for producing the water treatment adsorbents on a large scale.

Keywords: Carboxymethylated lignin, hybrid magnetic nanoparticles, heavy metal ions, ultrafast adsorption

1. Introduction

Water pollution by heavy metal ions has raised a global concern for the last few decades because of their rampant damage to the ecological environment. How to design a highly efficient and economic adsorbent for wastewater treatment is a challenging task to address due to enhanced industrial effluent discharges. Various adsorbents, such as carbon materials [1, 2], inorganic materials [3, 4], and biopolymers [5-7], have been developed for the adsorption of heavy metal ions from aqueous solutions. In an up-to-date research context, nanomaterials are regarded as the most promising novel adsorbents to remove heavy metal ions from wastewater because the unique physical and chemical properties of nanostructured adsorbents provide much higher efficiency and faster rates for the removal of heavy metal ions [8-10]. Among various nanostructured adsorbents, nanoparticles exhibit unprecedented opportunities for the adsorption of heavy metals ions in high efficiency [11, 12]. Especially, magnetic nanoparticles as well as their composites have emerged to draw considerable interests for the adsorption of heavy metal ions because of their intriguing features, such as easy separation of adsorbent and adsorbate by an external magnetic field, large surface area, uniform structure, and diversity in surface functionalization [3, 13-15]. The magnetic nanoparticles are used commonly as magnetic cores, which can be coated with a silica layer to enhance their chemical stability, as well as to avoid rapid oxidation and aggregation in the adsorption system of the heavy metal ions [16, 17]. Furthermore, the mesoporous silica shell surrounding the magnetic core allows the facile diffusion of heavy metal ions towards the binding sites through the pores and channel in it [18]. To improve the active sites for adsorbing heavy metal ions, the magnetic nanoparticles could be functionalized with various materials such as graphene oxide [19], carbon nanotubes [20] and polymers [21, 22] to produce functional hybrid nanomaterials. However, current adsorbents based on magnetic nanoparticles have certain limitations such as non-biodegradability, high-cost, and inferior adsorption capacity. There is still a challenge to

develop a technically and economically feasible route for large-scale commercial production of adsorbents with high removal capacity and high removal efficiency.

Lignin is one of the most abundant renewable aromatic polymers in nature, and tens of million tons of lignin are generated as a byproduct from the pulping industry on annual basis [23, 24]. It has been considered as a potential substitute of fossil fuels for the development of new materials or fine chemicals due to the low-cost, natural degradability and low toxicity [25, 26]. Lignin is abundant with various functional groups, especially phenol hydroxyl and carboxyl groups, which make it or its derivatives a promising raw material for preparing low cost adsorbents for heavy metal ions [27-29]. Recently, several studies have been reported to investigate lignin-based composites as novel biodegradable adsorbents for water and wastewater treatment, such as lignosulfonate-modified graphene hydrogel [30], poly (ethyleneimine)-graft-lignin [31], lignin-based resin [32] and lignin-grafted biopolymers [33, 34]. However, such lignin-based adsorbents often suffered from consuming relatively long time to reach adsorption equilibrium, mostly more than 2 h. An efficient way to tackle this problem is to establish more active sites to the lignin structure by various modification approaches. A great deal of work has reported modified lignins by introducing oxygen-, nitrogen-, or sulfur-containing functional groups for improved adsorption capacity of the pollutants. Only in very recent years, composite adsorbent based on modified lignin with various kind of nanomaterials, such as carbon nanotubes, graphene and TiO_2 nanoparticles, have been actively exploited to meet the challenging criteria of an efficient and green absorbent [35, 36].

Herein, novel eco-friendly and cost-effective hybrid nanoparticles were prepared with the aim of obtaining a high-efficiency adsorbent based on a magnetic core and mesoporous silica shell conjugated with the modified lignin (Scheme 1). To improve their active sites, numerous carboxylate groups were introduced to the lignin structure *via* carboxymethylation. Moreover, the carboxymethlated lignin was further functionalized by chemically cross-linking of the

magnetic mesoporous silica nanoparticles with epichlorohydrin (ECH), which increased their insolubility in water. Importantly, the adsorption capacity and adsorption kinetics of the magnetic lignin-based hybrid nanoparticles for the removal of heavy metal ions were determined. Besides, the adsorption mechanism was also further revealed in detail. We envision that this work reported here could open windows of opportunity not only for the valorization of industrial lignin, but also for the ultrafast removal of heavy metal ions from wastewater on a large scale.

2. Materials and Methods

2.1. Material

The organosolv lignin, i.e. formic acid lignin (FL), used in the present work was obtained from formic acid rapid-fractionation of bamboo (*Neosinocalamus affinis*) as previously reported [37]. Briefly, this lignin was extracted by one-step formic acid fractionation at 145 ºC for 45 min with a liquid to solid ratio of 7:1(mL/g). When the reactions were finished, the spent liquor was obtained by filtration and then 10 volumes of water were poured into the liquor to precipitate the dissolved lignin. The crude lignin was separated by centrifugation and washed with water twice at room temperature. Before use, the lignin purification process was conducted according to the method proposed by Zhang et al. [27]. Tetraethoxysilane (TEOS), 3-(aminopropyl)triethoxysilane (APTES), epichlorohydrin (ECH), monochloroacetic acid toluene, ethanol and were obtained from Sigma-Aldrich Company. Dialysis membrane (Cut off of 1000 g/mol) was obtained from Spectrum-Labs. All chemicals were analytical grade and used without further purification.

2.2 Synthesis of amine-functionalized Fe_3O_4@SiO_2

The magnetic particles were prepared by the combination of an oxidation–coprecipitation method and a chemical coprecipitation method as reported previously [38]. 100 mg of Fe_3O_4 particles were dispersed in a mixture solution containing 400 mL ethanol and 100 mL water

with 30 min sonication, and then the mixture was stirred for 30 min at room temperature.

After the pH was adjusted to 10 with $NH_3 \cdot H_2O$, TEOS (1 mL) was added into the suspension and stirred for 6 h. The resulting product was collected by magnetic separation and successively washed with ethanol and water several times, and then redispersed in dry toluene (300 mL). APTES (2 mL) was added dropwise and stirred for 24 h at room temperature. The obtained product (denoted as $Fe_3O_4@SiO_2–NH_2$) was separated using a magnet, washed three times with ethanol and dried using vacuum freeze-drying.

2.3 Preparation of carboxymethylated lignin

Carboxymethylated lignin was prepared according to the literature with a slight modification [39]. For that, 5 g of lignin was dispersed in 135 mL of methanol (72%) and then 13.5 mL of NaOH solution (30% w/v) was added dropwise, during 30 min under continuous stirring. After stirring for 90 min at room temperature, 6.0 g monochloroacetic acid was gradually added, and then the mixture was heated to 55 °C and stirred for 210 min. The mixture was filtered and placed into dialysis membranes and sealed. The membranes were put into deionized water for 2 days while water was replaced twice a day. Finally, the modified formic acid lignin (MFL) was dried using vacuum freeze-drying.

2.4 Preparation of lignin-based hybrid magnetic nanoparticles

In a typical procedure, 1.2 g carboxymethylated lignin was dissolved in 12 mL of NaOH solution (12% w/v) under mechanical stirring to form a clear solution. Next, the $Fe_3O_4@SiO_2$-NH_2 nanoparticles (0.4 g) were dispersed into 200 mL toluene with 30 min sonication, and then the suspension was added in the above solution. 8 mL ECH solution was dropwise added into the above dispersion and reacted at 70 °C for 3 h. Finally, the resulting modified lignin-based hybrid magnetic nanoparticles ($Fe_3O_4@SiO_2$-NH-MFL) were separated by a magnet, rinsed with ethanol, and dried using vacuum freeze-dryer.

As a control experiment, non-silica coated modified lignin-based hybrid magnetic

nanoparticles (Fe_3O_4-NH-MFL) and non-modified lignin-based hybrid magnetic nanoparticles (Fe_3O_4@SiO_2-NH-FL) were also prepared using the same procedure.

2.5 Characterizations

Fourier transform infrared spectroscopy (FTIR) was recorded by Thermo ScientificTM NicoletTM iSTM 50 FTIR Spectrometer (United States). Each spectrum was collected with ATR mode in the transmittance or absorbance mode from an accumulation of 64 scans in the range of resolution from 400 to 4000 cm^{-1} with a resolution of 4 cm^{-1}. Powder X-ray diffraction (XRD) patterns were recorded on an X-ray diffractometer (Bruker Discover D8, Germany) with Cu Kα radiation (λ=1.5418 Å). The zeta potentials were measured using a Zetasizer Nano ZS instrument (Malvern Instruments Ltd., UK). The ^{31}P-NMR experiments were performed at 298 K on a Bruker AVANCE III spectrometer operating at 202.5 MHz using a 5 mm Z-gradient BBO (Broadband Observe) cryo-probe. X-ray photoelectron spectroscopy (XPS) data was obtained with an ESCA Lab220i-XL electron spectrometer from VG Scientific using 300 W Al Kα radiation. The surface morphologies and chemical composition of samples were investigated by use of a scanning electron microscope (SEM; Zeiss SUPRA 55) with an accelerating voltage of 20 kV, combined with energy-dispersive X-ray spectroscopy (EDX). TEM measurements were carried out on a JEM-1400 Plus TEM microscope (JEOL Ltd., Japan) with an accelerating voltage of 80 kV.

2.6 Adsorption measurements

The adsorption capacities of the lignin-based hybrid magnetic nanoparticles were evaluated by the adsorption of heavy metal ions: Pb^{2+} and Cu^{2+}. The Pb^{2+} and Cu^{2+} aqueous solutions were prepared by dissolving $Pb(NO_3)_2$ and $CuSO_4 \cdot 5H_2O$ in deionized water and further diluted with deionized water to a desired concentration (50 mg/L for pH and contact time influence, while 10–150 mg/L with an increment of 10 mg/L for isotherms study). Generally, the experiments were carried out in a batch model described as follows: 20 mg of

freeze-dried adsorbent material was mixed with 40 mL metal ion solution and continuously stirred at 180 rpm. The initial solution pH values ranging from 2.0 to 6.0 were adjusted by adding a small quantity of 2.0 mol/L of HNO_3 or 1.0 mol/L of NaOH aqueous solution and measured with a pH meter. For pH influence and isotherms study, the mixture was stirred for 12 h to reach adsorption equilibrium. After filtration through a 0.22 mm membrane, metal ion concentrations of the filtrate were quantitatively measured using an atomic absorption spectrometer (AAS6300 Shimadzu). The adsorbed amount of metal ions was calculated according to the following Eq. (1),

$$q_t = (C_0 - Ct)V/m \quad (1)$$

where q_t is the adsorbed amount after time t; C_0 (mg/L) and C_t (mg/L) are initial concentration and concentration of the adsorbate after time t, respectively; V (L) is the volume of the solution, and m (g) is the weight of the adsorbent material used. All the experiments were performed in duplicate. Each point denotes an average value of duplicate measurements.

3. Results and discussion

3.1 Characterization

A schematic illustration of the synthetic route is depicted in Scheme 1. The magnetic hybrid nanoparticles were synthesized through a chemical cross-linking reaction between the amine-functionalized Fe_3O_4@SiO_2 and the carboxymethylated lignin.

The presence of magnetic nanoparticles as a core in the hybrid nanoparticles was investigated by XRD from 5° to 80° 2θ. As shown in Fig. 1a, the characteristic diffraction peaks at about 30.3°, 35.7°, 43.3°, 53.5°, 57.4° and 62.9° 2θ could be assigned to the [220], [311], [400], [422], [511] and [440] planes of magnetite (JCPDS card No. 19-0629), respectively. It is confirmed that the Fe_3O_4 nanoparticles have a hexagonal phase structure [40]. These peaks are all observed for the samples of amine-functionalized Fe_3O_4@SiO_2 and as-synthesized hybrid nanoparticles, indicating that the silica coating, further modification with amine groups and the

cross-linking reaction with lignin did not result in any significant change of the size and crystal structure of the Fe_3O_4 nanoparticles.

The FTIR technique was employed to identify the functional groups in the synthesized magnetic hybrid nanoparticles. As shown in Fig. 1b, it was found that the typical characteristic peaks of the carboxymethylated lignin at 3430 and 1600 cm^{-1} are ascribed to hydroxyl groups and carboxylate groups (asymmetric stretching), respectively [41]. The stretching bands at 1513 and 1452 cm^{-1} are due to aromatic rings, and the peaks at 1220 cm^{-1} could be ascribed to phenolic C-O groups [31]. Furthermore, the typical absorption peak for amine-functionalized Fe_3O_4@SiO_2 nanoparticles at 540 cm^{-1} is attributed to the stretching vibration of Fe-O bond, and the strong absorption peaks at 1064 cm^{-1} result from Si-O vibrations, which highlighted the formation silica network surrounded the Fe_3O_4 nanoparticle core [18]. Two weak peaks at 1640 and 1566 cm^{-1} are attributed to the deformation vibration of amide I and amide II, respectively, indicating the successful amine modification of Fe_3O_4@SiO_2 nanoparticles [31]. After chemical cross-linking between carboxymethylated lignin and amine-functionalized Fe_3O_4@SiO_2 nanoparticles, these peaks are clearly found in the magnetic hybrid nanoparticles. Additionally, the XPS clearly confirms that the Fe_3O_4@SiO_2-NH-MFL nanoparticles are composed of C, O, Fe, Si, and N (see Fig. 1c and d). Based on the above comprehensive analysis, we conclude the successful combination of amine-functionalized Fe_3O_4@SiO_2 nanoparticles by the carboxymethylated lignin in the end product. The linkage of modified lignin with magnetic nanoparticles not only facilitated heavy metal ion removal, but also improved the hydrophilicity of the adsorbents, which contributed positively to enhanced interactions between the adsorbents and the adsorbates.

The morphology and structure of the synthesized nanoparticles were observed by TEM and SEM equipped with an EDX system. As shown in Fig. 2a-d and Fig. S1a-d, the obtained Fe_3O_4, Fe_3O_4@SiO_2 and that of amine-functionalized nanoparticles, as well as the

Fe_3O_4@SiO_2-NH-MFL nanoparticles present an approximate diameter of 10-20 nm and a nearly spherical shape. After the silica-coating process, further amine modification and the cross-linking reaction with modified lignin, the as-synthesized nanoparticles display a relatively similar spherical morphology and size, indicating that these functionalization processes did not result in any further agglomeration. The morphology of these nanoparticles was also examined by SEM, as displayed in Fig. $2a_1$-d_1, which agreed well with the result found by TEM. Representative morphologies of the as-synthesized Fe_3O_4@SiO_2-NH-MFL nanoparticles structures, as revealed by SEM (Fig. $2d_1$), exhibit a coarse and polydisperse mesoporous aggregate structure, which enables the synthesized hybrid nanoparticles to deliver a high adsorption capability for heavy metal ions owing to a larger exposed specific surface area. The EDX spectrum (Fig. S2a) shows that the C, O, Fe, Si, and N are the main elements in the Fe_3O_4@SiO_2-NH-MFL nanoparticles. Compared with amine-functionalized Fe_3O_4@SiO_2 (see Fig. S2b), the C and O contents are remarkably higher in the synthesized hybrid nanoparticles, indicating the successful combination between carboxymethylated lignin and amine-functionalized Fe_3O_4@SiO_2 nanoparticles.

In order to obtain the information about the surface charge of synthesized nanoparticles and the stability of liquid dispersions, zeta potential was measured at different pH values. As shown in Fig. 3a, the zeta potential of synthesized hybrid nanoparticles (Fe_3O_4@SiO_2-NH-MFL) decreased with increasing pH, and the isoelectric point was reached at pH 2.4. At pH > 3, the hybrid nanoparticles possess a negative surface charge of below -30 mV. In comparison, the isoelectric point of Fe_3O_4@SiO_2-NH-FL and Fe_3O_4@SiO_2-MFL shifted to 3.5 and 3.1, respectively, and then the surface charge transformed to a negative charge with large fluctuations. These results indicate that the synthesized hybrid nanoparticles (Fe_3O_4@SiO_2-NH-MFL) dispersion exhibited excellent stability over a wide pH range. The presence of coated silica and linked carboxymethylated lignin did have a clear effect on the zeta potential of hybrid

nanoparticles (Fe_3O_4@SiO_2-NH-MFL) [42]. As shown in Table 1, the carboxymethylation of lignin resulted in a dramatic increase in the content of carboxylic groups (1.26 mmol/g) as compared to the raw lignin (0.47 mmol/g). More importantly, the large amount of carboxylate groups on the surface of our hybrid nanoparticles could provide more and stronger chelating sites for heavy metal ions [42]. The synthesized hybrid nanoparticles in a water dispersion after the adsorption of Pb^{2+} showed rapid movement to the applied magnetic field in 20 s and were able to be re-dispersed easily with a slight shake once the magnetic field was removed (Fig. 3b). It is suggested that the hybrid nanoparticles exhibited superior performance in magnetic properties, which was an advantage for their applications.

3.2 Adsorption performance

In general, the pH value is considered as an important factor affecting both the speciation of metal ions and the surface charge of the adsorbent, and thus influence the adsorption process at the water–solid interface [31]. Fig. 4a and b show the effect of initial pH on the adsorption capacity of Pb^{2+} and Cu^{2+} on Fe_3O_4@SiO_2-NH-MFL, Fe_3O_4@SiO_2-NH-FL and Fe_3O_4@SiO_2-MFL. In this work, the effect of pH values was investigated in the range of 2.0 and 6.0 because of the probability of the formation of metal precipitation for Pb^{2+} and Cu^{2+} ions at higher pH values. It could be seen that the adsorption capacities of Pb^{2+} and Cu^{2+} ions on these three adsorbents were highly pH-dependent. In the case of Fe_3O_4@SiO_2-NH-MFL, the level of heavy metal ions adsorption increased more dramatically with increasing pH in the range of 3–5. The capacity is nearly zero for Pb^{2+} ions at pH $\leq$ 2 and for Cu^{2+} ions at pH $\leq$ 2.5, respectively. This is probably due to the protonation of the carboxylic acid groups and hydroxyls at low pH values, and a competitive adsorption between H^+ ions and metal ions in the solution. As the pH increased, the ionization enhanced the electric attraction between cationic metal ions and negatively charged adsorbent surface, leading to a greater adsorption of heavy metal ions. This was highly in agreement with the analysis of the zeta potential for the adsorbents. In contrast,

both Fe_3O_4@SiO_2-NH-FL and Fe_3O_4@SiO_2-MFL nanoparticles exhibited lower levels of adsorption than Fe_3O_4@SiO_2-NH-MFL for Pb^{2+} and Cu^{2+} ions in the entire pH ranges studied. The obvious discrepancy in the metal ions removal, in which Fe_3O_4@SiO_2-NH-MFL demonstrated enhanced removal capacities for Pb^{2+} and Cu^{2+} in compared with the Fe_3O_4@SiO_2-NH-FL and Fe_3O_4@SiO_2-MFL, may be attributed to two following aspects. On one hand, the decoration of the coated silica on the magnetic cores enhanced the adsorption performance of hybrid nanoparticles (Fe_3O_4@SiO_2-NH-MFL). On the other hand, the cross-linked carboxymethylated lignin offered a large amount of carboxylate groups on the hybrid nanoparticles surface and thus the active sites in adsorbent were increased, leading to a stronger adsorption.

Conveniently, pH value of 5.0 was selected in the following experiments to further investigate the adsorption of hybrid nanoparticles (Fe_3O_4@SiO_2-NH-MFL). Fig. 4c and d show the removal of Pb^{2+} and Cu^{2+} ions by the synthesized hybrid nanoparticles (Fe_3O_4@SiO_2-NH-MFL) as a function of contact time. Impressively, the adsorption of Pb^{2+} and Cu^{2+} ions on the Fe_3O_4@SiO_2-NH-MFL nanoparticles is a very quick process and the equilibrium could be achieved within 30 s when an initial metal ions content concentration of 50 mg/L was studied. Such an ultrafast adsorption of heavy metal ions by hybrid nanoparticles holds a greater potential to meet the practical applications. This superior performance of the adsorbent can be attributed to the following synergistic effects: (1) the cross-linked carboxymethylated lignin could provide numerous active sites, which have high affinity with Pb^{2+} and Cu^{2+}, (2) the porous structure of the magnetic hybrid nanoparticles offers a large surface area for absorbents being in contact; (3) the highly negative charge on the hybrid nanoparticle surface ($\zeta < -30$ mV in the pH range of 3–11) could accelerate the diffusion and enrichment of metal ions from the aqueous solution towards the surface of the synthesized material.

The lignin-based adsorbents were reported to have the adsorption equilibration time of 20–

240 min for Pb^{2+} or Cu^{2+}, as summarized in Table 2. The adsorption equilibrium efficiency observed in the current work is much faster than the reported values, indicating an ultrafast adsorption of the as-synthesized lignin-based hybrid magnetic nanoparticles.

The Pb^{2+} and Cu^{2+} adsorption isotherms were also investigated by varying the initial ion concentrations from 10 to 200 mg/L with a constant adsorbent dosage of 0.5 g/L. As shown in Fig. 4e and f, the adsorption capacities of hybrid nanoparticles (Fe_3O_4@SiO_2-NH-MFL) at first increased rapidly at low metal ion concentration of Pb^{2+} and Cu^{2+} and the adsorption reached a plateau when the initial ion concentration went beyond 80 mg/L for Pb^{2+} and 50 mg/L for Cu^{2+}. The maximum adsorption was as high as 152.4 and 71.4 mg/L for Pb^{2+} and Cu^{2+}, respectively. The excellent adsorption capacities for Pb^{2+} and Cu^{2+} are ascribed to a large amount of negatively charged functional groups, such as $–COO^-$ and -OH on the surface of the lignin-based hybrid magnetic nanoparticles and the unique mesoporous structure, which endowed extensively exposed surface to form abundant adsorption sites for metal ion capture.

The adsorption isotherms were further investigated by Langmuir (eqn (2)), Freundlich (eqn (3)) and Sips (eqn (4)) adsorption models, which were given by the following equations [54-56]:

$$q_e = q_m K_L C_e/(1+K_L C_e) \quad (2)$$

$$q_e = K_F C_e^{1/n} \quad (3)$$

$$q_e = q_s K_s C_e^m/(1+K_s C_e^m) \quad (4)$$

where C_e (mg/L) and q_e (mg/g) are metal ion concentration and adsorption capacity at equilibrium, respectively. q_m represents the maximum adsorption capacities of metal ions (mg/g). K_L is the Langmuir adsorption constant. K_F is the Freundlich constant indicating the adsorption capacity, n is the heterogeneity factor representing the adsorption intensity. In the Sips model, q_s is the specific adsorption capacity at saturation, mg/g, K_S is Sips isotherm constant, mL/mg, and m is the heterogeneity factor.

As shown in Fig. 4e and f, the experimental data for the adsorption of Pb^{2+} could be fitted by the Langmuir and Sips models with the correlation coefficient of 0.8298 and 0.8385, respectively. In the case of Cu^{2+} adsorption, the Sips model also fits the experimental data well with a higher correlation coefficient (R^2 = 0.9369), as compared with that obtained by the Langmuir and (R^2 = 0.8842) and Freundlich isotherm model (R^2 = 0.7936). These results indicate that the Sips model offers the best description for the adsorption of both Pb^{2+} and Cu^{2+} onto the synthesized Fe_3O_4@SiO_2-NH-MFL nanoparticles. With the use of the Sips model, the maximum adsorption capacity was determined to be 150.33 and 70.69 mg/g for Pb^{2+} and Cu^{2+} ions, respectively. The Fe_3O_4@SiO_2-NH-MFL nanoparticles also showed a relatively high adsorption capacity for Pb^{2+} and Cu^{2+} ions among various lignin-based adsorbents (Table 2). Therefore, the as-synthesized magnetic hybrid nanoparticles are a high-efficiency adsorbent for the removal of heavy metal ions from aqueous solutions. To explore the regeneration and reuse performance of Fe_3O_4@SiO_2-NH-MFL nanoparticles, adsorption-desorption experiments of heavy metal ions were conducted. Unfortunately, it was found that only 40.89% and 44.33% of adsorbents, after the adsorption of Pb^{2+} and Cu^{2+} respectively, could be recovered from the desorption process with 1 M HCl. In the case of 0.1 M HCl, 62.07% and 46.69% of adsorbents could be recovered after the adsorption of Pb^{2+} and Cu^{2+}, respectively. The low recovery rate is thought to be ascribed to the low pH-stability of Fe_3O_4 nanoparticles at strong acidic conditions.

3.3 Adsorption mechanism

To study the adsorption mechanism of the heavy metal ion onto the Fe_3O_4@SiO_2-NH-MFL nanoparticles, its FTIR analysis was carried out before and after adsorption (Fe_3O_4@SiO_2-NH-MFL+Pb), as shown in Fig. 5a. After adsorption of Pb^{2+}, the stretching vibration of the -OH group shifted from 3369 to 3302 cm^{-1}, indicating that strong -OH interactions are developed after Pb^{2+} adsorption, which can be ascribed to the hydrogen bonding between -OH groups contained in the modified lignin structure. Furthermore, the C=O stretching vibration in the -

COO^- groups resulted in a slight shift from 1712 to 1706 cm^{-1} and decreased the relative intensity of the C=O absorption band after the Pb^{2+} adsorption. The adsorption capacity can be attributed to the abundant surface functional groups, including -OH and $–COO^-$ on the lignin-based hybrid magnetic nanoparticles, which can offer many adsorption active sites toward heavy metal ions.

To further elucidate the sorption mechanism of Pb^{2+} ions on the as-synthesized hybrid nanoparticles, XPS was applied to analyze before and after adsorption of Pb^{2+} (Fig 5b). After the metal ion adsorption, the relative area ratio for the peak attributed to Na 1s decreased from 2.0 to 1.2, instead some characteristic peaks about Pb were observed in the XPS spectra of Fe_3O_4@SiO_2-NH-MFL+Pb, which indicated that ion exchange between –COONa and Pb^{2+} contributed to the metal ions adsorption. These results confirmed that the $-COO^-$ groups on the adsorbent surface play a primary role in the adsorption process. Moreover, the high-resolution XPS scan was carried out to analyze the bonding types of element C and O on the Fe_3O_4@SiO_2-NH-MFL surface before and after metal ions adsorption. As shown in Fig. 5c and d, the peak of the C 1s at 286.06 eV was attributable to C-O and the peak at 287.33 eV was attributable to $–COO^-$. After the metal ions adsorption, the C-O signal shifted to lower binding energy at 285.89 eV, which was probably caused by the interaction of Pb^{2+} ions with C-OH, while the peak for the $–COO^-$ signal shifted to higher binding energy from 287.33 eV to 287.72 eV, which was due to the binding of Pb ions to $–COO^-$ [57]. As shown in Fig. 5e and f, the O 1s spectra of Fe_3O_4@SiO_2-NH-MFL nanoparticles were split into three overlapped peaks, including the metal oxides signal at 530.45 eV, the –OH signal at 532.77 eV and the $–COO^-$ signal at 534.90 eV. After the metal ions adsorption, the peak which was attributed to –OH shifted to lower binding energy from 532.77 eV to 532.27 eV and the peak of the $–COO^-$ signal shifted to higher binding energy due to the decreased electron density, which was feasibly caused by the interaction of Pb^{2+} ions with oxygen atoms. These results further confirmed that the –OH and

–COO^- groups on the Fe_3O_4@SiO_2-NH-MFL nanoparticles play a significant role in the ultrafast adsorption process. The C-OH could be involved in the adsorption of Pb^{2+} by the formation of Pb-OC bonding [31]. In addition, the morphologies of the Fe_3O_4@SiO_2-NH-MFL nanoparticles after adsorption as well as the EDX mapping results further confirmed that the Pb^{2+} was adsorbed on the surface of Fe_3O_4@SiO_2-NH-MFL nanoparticles (see Fig. S3). Therefore, based on the above discussions, the adsorption mechanism of heavy metal ions is mainly attributed to ion exchange and hydrogen bonding.

4. Conclusions

In this work, we have developed a highly efficient and effective bio-degradable adsorbent for heavy metal ion removal by cross-linking carboxymethylated lignin with a silica coated magnetic nanoparticles, Fe_3O_4@SiO_2-NH-MFL. Taking the advantages of their special mesoporous structure and numerous active sites, the as-synthesized hybrid nanoparticles were found to be exceptionally effective and efficient in the removal of heavy metal ions from aqueous solutions, with ultrafast adsorption equilibrium (within 30 s) and a relatively high adsorption capacity of 150.33 and 70.69 mg/g for Pb^{2+} and Cu^{2+} ions, respectively. The ion exchange and hydrogen bonding mainly contribute to the ultrafast and high capacity removal of heavy metal ions by Fe_3O_4@SiO_2-NH-MFL nanoparticles. All of these superior properties suggest that the Fe_3O_4@SiO_2-NH-MFL nanoparticles could become an eco-friendly and cost-effective hybrid materials for the ultrafast removal of heavy metal ions from wastewater on a large scale.

Acknowledgements

The authors would like to acknowledge financial support from the China Scholarship Council, the Graduate School of Chemical Engineering, Fortum Foundation, the National Natural Science Foundation of China (31370581 and 31540009), the Independent Innovation and Achievements Transformation Project of Shandong Province (2014CGZH0302), and the

Yellow River Mouth Scholar Program (DYRC20120105). We thank Jingxin Su for providing the support of XPS analysis software. This work is also part of the activities within the Johan Gadolin Process Chemistry Centre, a Center of Excellence appointed by Åbo Akademi University during 2015-2018. Also, NSERC and Canada Research Chair programs are acknowledged for supporting this research.

Appendix A. Supplementary data

Supplementary data associated with this article can be found, in the online version.

References

[1] S. Bolisetty, R. Mezzenga, Amyloid–carbon hybrid membranes for universal water purification, Nat. Nanotechnol 11 (2016) 365-371.

[2] J. Xu, Z. Cao, Y. Zhang, Z. Yuan, Z. Lou, X. Xu, X. Wang, A review of functionalized carbon nanotubes and graphene for heavy metal adsorption from water: Preparation, application, and mechanism, Chemosphere 195 (2018) 351-364.

[3] C.H. Yen, H.L. Lien, J.S. Chung, H.D. Yeh, Adsorption of precious metals in water by dendrimer modified magnetic nanoparticles, J. Hazard. Mater. 322 (2017) 215-222.

[4] M.K. Uddin, A review on the adsorption of heavy metals by clay minerals, with special focus on the past decade, Chem. Eng. J. 308 (2017) 438-462.

[5] E. Elgueta, J. Sánchez, D. Dax, C. Xu, S. Willför, B.L. Rivas, M. González, Functionalized galactoglucomannan-based hydrogels for the removal of metal cations from aqueous solutions, J. Appl. Polym. Sci. 133 (2016) 44093-44100.

[6] P. Kanmani, J. Aravind, M. Kamaraj, P. Sureshbabu, S. Karthikeyan, Environmental applications of chitosan and cellulosic biopolymers: A comprehensive outlook, Bioresour. Technol. 242 (2017) 295-303.

[7] D. Dax, M.S. Chávez, C. Xu, S. Willför, R.T. Mendonça, J. Sánchez, Cationic hemicellulose-based hydrogels for arsenic and chromium removal from aqueous solutions, Carbohydr Polym. 111 (2014) 797-805.

[8] R.E. Abouzeid, R. Khiari, N. El-Wakil, A. Dufresne, Current state and new trends in the use of cellulose nanomaterials for wastewater treatment, Biomacromolecules (2018) 573-597.

[9] J.E. Efome, D. Rana, T. Matsuura, C.Q. Lan, Insight studies on metal-organic framework nanofibrous membrane adsorption and activation for heavy metal ions removal from aqueous solution, ACS Appl. Mater. Interfaces 10 (2018) 18619-18629.

[10] Q. Yuan, P. Li, J. Liu, Y. Lin, Y. Cai, Y. Ye, C. Liang, Facet-dependent selective adsorption of Mn-doped α-Fe_2O_3 nanocrystals toward heavy-metal ions, Chem. Mater. 29 (2017) 10198-10205.

[11] T.V. Charpentier, A. Neville, J.L. Lanigan, R. Barker, M.J. Smith, T. Richardson, Preparation of magnetic carboxymethylchitosan nanoparticles for adsorption of heavy metal ions, ACS omega 1 (2016) 77-83.

[12] Q. Liu, F. Li, H. Lu, M. Li, J. Liu, S. Zhang, Q. Sun, L. Xiong, Enhanced dispersion stability and heavy metal ion adsorption capability of oxidized starch nanoparticles, Food Chem. 242 (2018) 256-263.

[13] H. Zhu, X. Tan, L. Tan, H. Zhang, H. Liu, M. Fang, T. Hayat, X. Wang, Magnetic porous polymers prepared via high internal phase emulsions for efficient removal of Pb^{2+} and Cd^{2+}. ACS Sustain. Chem. Eng. 6 (2018) 5206-5213.

[14] Y. Cai, C. Li, D. Wu, W. Wang, F. Tan, X. Wang, P.K. Wong, X. Qiao, Highly active MgO nanoparticles for simultaneous bacterial inactivation and heavy metal removal from aqueous solution, Chem. Eng. J. 312 (2017) 158-166.

[15] J. Wu, H.S. Zhu, G. Liu, L.Q. Tan, X.Y. Hu, C.L. Chen, N.S. Alharbi, T. Hayat, X.L. Tan, Fabrication of core-shell CMNP@PmPD nanocomposite for efficient As(V) adsorption and reduction, ACS Sustain. Chem. Eng. 5 (2017) 4399–4407.

[16] B. Mu, A. Wang, One-pot fabrication of multifunctional superparamagnetic attapulgite/Fe_3O_4/polyaniline nanocomposites served as an adsorbent and catalyst support, J. Mater. Chem. A 3 (2015) 281-289.

[17] R. Roto, Y. Yusran, A. Kuncaka, Magnetic adsorbent of Fe_3O_4@SiO_2 core-shell nanoparticles modified with thiol group for chloroauric ion adsorption, Appl. Surf. Sci. 377 (2016) 30-36.

[18] M.S. Moorthy, D.J. Seo, H.J. Song, S.S. Park, C.S. Ha, Magnetic mesoporous silica hybrid nanoparticles for highly selective boron adsorption, J. Mater. Chem. A 1 (2013) 12485-12496.

[19] A. Sherlala, A. Raman, M. Bello, A. Asghar, A review of the applications of organo-functionalized magnetic graphene oxide nanocomposites for heavy metal adsorption, Chemosphere 193 (2018) 1004-1017.

[20] Y. Wang, L. Hu, G. Zhang, T. Yan, L. Yan, Q. Wei, B. Du, Removal of Pb (II) and methylene blue from aqueous solution by magnetic hydroxyapatite-immobilized oxidized multi-walled carbon nanotubes, J. Colloid Interface Sci. 494 (2017) 380-388.

[21] H.L. Fan, S.F. Zhou, W.Z. Jiao, G.S. Qi, Y.Z. Liu, Removal of heavy metal ions by magnetic chitosan nanoparticles prepared continuously via high-gravity reactive precipitation method, Carbohydr Polym. 174 (2017) 1192-1200.

[22] F. Ge, M.M. Li, H. Ye, B.X. Zhao, Effective removal of heavy metal ions Cd^{2+}, Zn^{2+}, Pb^{2+}, Cu^{2+} from aqueous solution by polymer-modified magnetic nanoparticles, J. Hazard. Mater. 211 (2012) 366-372.

[23] T. Aro, P. Fatehi, Production and application of lignosulfonates and sulfonated lignin, ChemSusChem 10 (2017) 1861-1877.

[24] F. Kong, S. Wang, J.T. Price, M.K. Konduri, P. Fatehi, Water soluble kraft lignin–acrylic acid copolymer: Synthesis and characterization, Green Chem. 17 (2015) 4355-4366.

[25] R.L. Couch, J.T. Price, P. Fatehi, Production of flocculant from thermomechanical pulping lignin via nitric acid treatment, ACS Sustain. Chem. Eng. 4 (2016) 1954-1962.

[26] M.K. Konduri, P. Fatehi, Production of water-soluble hardwood Kraft Lignin via Sulfomethylation using formaldehyde and sodium sulfite, ACS Sustain. Chem. Eng. 3 (2015) 1172-1182.

[27] Y. Zhang, Q. Hou, W. Xu, M. Qin, Y. Fu, Z. Wang, S. Willför, C. Xu, Revealing the structure of bamboo lignin obtained by formic acid delignification at different pressure levels, Ind. Crops Prod. 108 (2017) 864-871.

[28] Y. Zhang, M. Qin, W. Xu, Y. Fu, Z. Wang, Z. Li, S. Willför, C. Xu, Q. Hou, Structural changes of bamboo-derived lignin in an integrated process of autohydrolysis and formic acid inducing rapid delignification, Ind. Crops Prod. 115 (2018) 194-201.

[29] X. Guo, S. Zhang, X. Shan, Adsorption of metal ions on lignin, J. Hazard. Mater. 151 (2008) 134-142.

[30] F. Li, X. Wang, T. Yuan, R. Sun, A lignosulfonate-modified graphene hydrogel with ultrahigh adsorption capacity for Pb (II) removal, J. Mater. Chem. A 4 (2016) 11888-11896.

[31] E. Zong, G. Huang, X. Liu, W. Lei, S. Jiang, Z. Ma, J. Wang, P. Song, A lignin-based nano-adsorbent for superfast and highly selective removal of phosphate, J. Mater. Chem. A 6 (2018) 9971-9983.

[32] F.B. Liang, Y.L. Song, C.P. Huang, Y.X. Li, B.H. Chen, Synthesis of novel lignin-based ion-exchange resin and its utilization in heavy metals removal, Ind. Eng. Chem. Res. 52 (2013) 1267-1274.

[33] A.B. Albadarin, M.N. Collins, M. Naushad, S. Shirazian, G. Walker, C. Mangwandi, Activated lignin-chitosan extruded blends for efficient adsorption of methylene blue, Chem. Eng. J. 307 (2017) 264-272.

[34] P. Bartczak, Ł. Klapiszewski, M. Wysokowski, I. Majchrzak, W. Czernicka, A. Piasecki, H. Ehrlich, T. Jesionowski, Treatment of model solutions and wastewater containing selected hazardous metal ions using a chitin/lignin hybrid material as an effective sorbent, J. Environ. Manage. 204 (2017) 300-310.

[35] N. Supanchaiyamat, K. Jetsrisuparb, J.T. Knijnenburg, D.C. Tsang, A.J. Hunt, Lignin materials for adsorption: current trend, perspectives and opportunities, Bioresour. Technol. (2018).

[36] Y. Ge, Z. Li, Application of lignin and its derivatives in adsorption of heavy metal ions in water: a review, ACS Sustain. Chem. Eng. 6 (2018) 7181-7192.

[37] Y. Zhang, Q. Hou, Y. Fu, C. Xu, A.I. Smeds, S. Willför, Z. Wang, Z. Li, M. Qin, One-step fractionation of the main components of bamboo by formic acid-based organosolv process under pressure, J. Wood Chem. Technol. 38 (2018) 170-182.

[38] S. Zhang, Y. Zhou, W. Nie, L. Song, Preparation of Fe_3O_4/chitosan/poly (acrylic acid) composite particles and its application in adsorbing copper ion (II), Cellulose 19 (2012) 2081-2091.

[39] S. Li, J.A. Willoughby, O.J. Rojas, Oil-in-Water Emulsions Stabilized by Carboxymethylated Lignins: Properties and Energy Prospects, ChemSusChem 9 (2016) 2460-2469.

[40] F.Y. Cheng, C.H. Su, Y.S. Yang, C.S. Yeh, C.Y. Tsai, C.L. Wu, M.T. Wu, D.B. Shieh, Characterization of aqueous dispersions of Fe_3O_4 nanoparticles and their biomedical applications, Biomaterials 26 (2005) 729-738.

[41] Z. Li, Y. Ge, L. Wan, Fabrication of a green porous lignin-based sphere for the removal of lead ions from aqueous media, J. Hazard. Mater. 285 (2015) 77-83.

[42] Y. Ren, H.A. Abbood, F. He, H. Peng, K. Huang, Magnetic EDTA-modified chitosan/SiO_2/Fe_3O_4 adsorbent: preparation, characterization, and application in heavy metal adsorption, Chem. Eng. J. 226 (2013) 300-311.

[43] X. Liu, H. Zhu, C. Qin, J. Zhou, J.R. Zhao, S. Wang, Adsorption of heavy metal ion from aqueous single metal solution by aminated epoxy-lignin, BioResources 8 (2013) 2257-2269.

[44] C. Jin, X. Zhang, J. Xin, G. Liu, G. Wu, Z. Kong, J. Zhang, Clickable synthesis of 1, 2, 4-triazole modified lignin-based adsorbent for the selective removal of Cd (II), ACS Sustain. Chem. Eng. 5 (2017) 4086-4093.

[45] Y. Ge, Q. Song, Z. Li, A Mannich base biosorbent derived from alkaline lignin for lead removal from aqueous solution, J. Ind. Eng. Chem. 23 (2015) 228-234.

[46] Y. Ge, L. Qin, Z. Li, Lignin microspheres: An effective and recyclable natural polymer-based adsorbent for lead ion removal, Mater. Design 95 (2016) 141-147.

[47] L. Qin, Y. Ge, B. Deng, Z. Li, Poly (ethylene imine) anchored lignin composite for heavy metals capturing in water, J. Taiwan Inst. Chem. Eng. 71 (2017) 84-90.

[48] Z. Li, Y. Kong, Y. Ge, Synthesis of porous lignin xanthate resin for Pb^{2+} removal from aqueous solution, Chem. Eng. J. 270 (2015) 229-234.

[49] Y. Ge, Z. Li, Y. Kong, Q. Song, K. Wang, Heavy metal ions retention by bi-functionalized lignin: Synthesis, applications, and adsorption mechanisms, J. Ind. Eng. Chem. 20 (2014) 4429-4436.

[50] F. Ciesielczyk, P. Bartczak, Ł. Klapiszewski, T. Jesionowski, Treatment of model and galvanic waste solutions of copper (II) ions using a lignin/inorganic oxide hybrid as an effective sorbent, J. Hazard. Mater. 328 (2017) 150-159.

[51] Ł. Klapiszewski, K. Siwińska-Stefańska, D. Kołodyńska, Development of lignin based multifunctional hybrid materials for Cu (II) and Cd (II) removal from the aqueous system, Chem. Eng. J. 330 (2017) 518-530.

[52] Z. Li, J. Chen, Y. Ge, Removal of lead ion and oil droplet from aqueous solution by lignin-grafted carbon nanotubes, Chem. Eng. J. 308 (2017) 809-817.

[53] W.S. Peternele, A.A. Winkler-Hechenleitner, E.A.G. Pineda, Adsorption of Cd(II) and Pb(II) onto functionalized formic lignin from sugarcane.bagasse, Bioresour. Technol. 68 (1999) 95–100.

[54] X. Wang, J. Cai, Y. Zhang, L. Li, L. Jiang, C. Wang, Heavy metal sorption properties of magnesium titanate mesoporous nanorods, J. Mater. Chem. A 3 (2015) 11796-11800.

[55] X. Ge, X. Song, Y. Ma, H. Zhou, G. Wang, H. Zhang, Y. Zhang, H. Zhao, P.K. Wong, Fabrication of hierarchical iron-containing MnO_2 hollow microspheres assembled by thickness-tunable nanosheets for efficient phosphate removal, J. Mater. Chem. A 4 (2016) 14814-14826.

[56] Q. Xu, Y. Wang, L. Jin, Y. Wang, M. Qin, Adsorption of Cu (II), Pb (II) and Cr (VI) from aqueous solutions using black wattle tannin-immobilized nanocellulose, J. Hazard. Mater. 339 (2017) 91–99.

[57] M. Zhang, L. Song, H. Jiang, S. Li, Y. Shao, J. Yang, J. Li, Biomass based hydrogel as an adsorbent for the fast removal of heavy metal ions from aqueous solutions, J. Mater. Chem. A 5 (2017) 3434-3446.

Figure captions

Scheme 1 A schematic process flow diagram illustrating the synthesis of the lignin-based hybrid magnetic nanoparticles.

Fig. 1. (a) XRD patterns and (b) FTIR spectra of synthesized nanoparticles. XPS survey spectra of (c) MFL and (d) Fe_3O_4@SiO_2-NH-MFL.

Fig. 2. Representative TEM images (left column) and SEM images (right column) of Fe_3O_4 (a and a_1), Fe_3O_4@SiO_2 (b and b_1), Fe_3O_4@SiO_2-NH_2 (c and c_1) and Fe_3O_4@SiO_2-NH-MFL (d and d_1).

Fig. 3. (a) ζ-potentials of the synthesized nanoparticles as a function of pH. (b) The separation of Fe_3O_4@SiO_2-NH-MFL nanoparticles from suspension under an external magnetic field.

Fig. 4. (a) Effect of pH on the adsorption capacities of Pb^{2+} and (b) Cu^{2+} by Fe_3O_4@SiO_2-NH-MFL, Fe_3O_4@SiO_2-NH-FL and Fe_3O_4@SiO_2-MFL. (c) Effect of contact time on the adsorption capacity of Pb^{2+} and (d) Cu^{2+} by Fe_3O_4@SiO_2-NH-MFL. (e) Adsorption isotherms for Pb^{2+} and (f) Cu^{2+} adsorption on Fe_3O_4@SiO_2-NH-MFL and the corresponding Langmuir, Freundlich and Sips models.

Fig. 5. FTIR analysis (a), XPS survey spectra (b), O 1s spectra (c and d) and C 1s spectra (e and f) of Fe_3O_4@SiO_2-NH-MFL before and after the adsorption of Pb^{2+} ions.

Table 1 Quantification of the hydroxyl and carboxyl groups of the lignin before (FL) and after (MFL) carboxymethylation by quantitative ^{31}P NMR method (mmol/g).

Lignin sample	Aliphatic OH	Phenolic OH			Total OH	Carboxylic acid
		Syringyl	Guaiacyl	*p*-Hydroxyl		
FL	1.24	1.61	0.97	0.95	4.58	0.47
MFL	1.28	1.45	0.85	0.84	4.42	1.26

Table 2 Comparison of heavy metals adsorption capacities in water of Fe_3O_4@SiO_2-NH-MFL nanoparticles with other lignin-based adsorbents in the literature.

Adsorbent	Equilibrium time (min)	Adsorption capacity ($mg\ g^{-1}$)		Ref.
		Pb^{2+}	Cu^{2+}	
Porous lignin-based sphere	150	27.1	-	[41]
Aminated epoxy-lignin	50	72.48	55.35	[43]
Lignin-triazole	180	42	18	[44]
Alkaline lignin grafted with methylamine	60	60.5	-	[45]
Poly(ethylenimine)-grafted lignin microspheres	at least 60 min	33.9	-	[46]
Poly(ethylenimine)-grafted lignin	50	-	98.0	[47]
Lignin xanthate resin	180	64.9	-	[48]
Lignin-DETA-SO_3	60	53.8	45.4	[49]
Lignin-chitin hybird	30	75.7	91.7	[34]
MgO-SiO_2-lignin hybrid	60	-	83.9	[50]
TiO_2-SiO_2/lignin hybrid	20-30	59.9	-	[51]
TiO_2/lignin hybrid	20-30	35.7	-	[51]
Lignosulfonate-graphene hydrogel	240	1210	-	[30]
Lignin grafted carbon nanotubes	40-50	235	-	[52]
Carboxymethylated lignin	480	135.17	-	[53]
Fe_3O_4@SiO_2-NH-MFL nanoparticles	0.5	150.33	70.7	Present study

Scheme 1 A schematic process flow diagram illustrating the synthesis of the lignin-based hybrid magnetic nanoparticles.

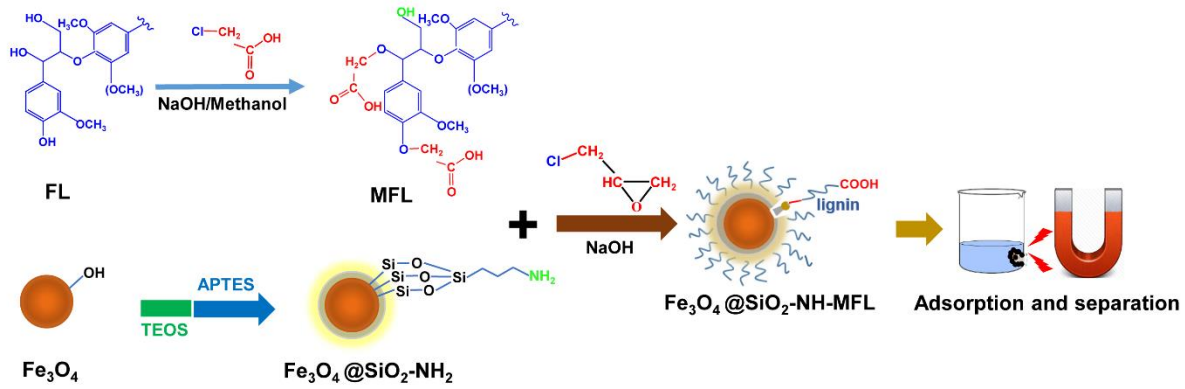

Fig. 1. (a) XRD patterns and (b) FTIR spectra of synthesized nanoparticles. XPS survey spectra of (c) MFL and (d) Fe_3O_4@SiO_2-NH-MFL.

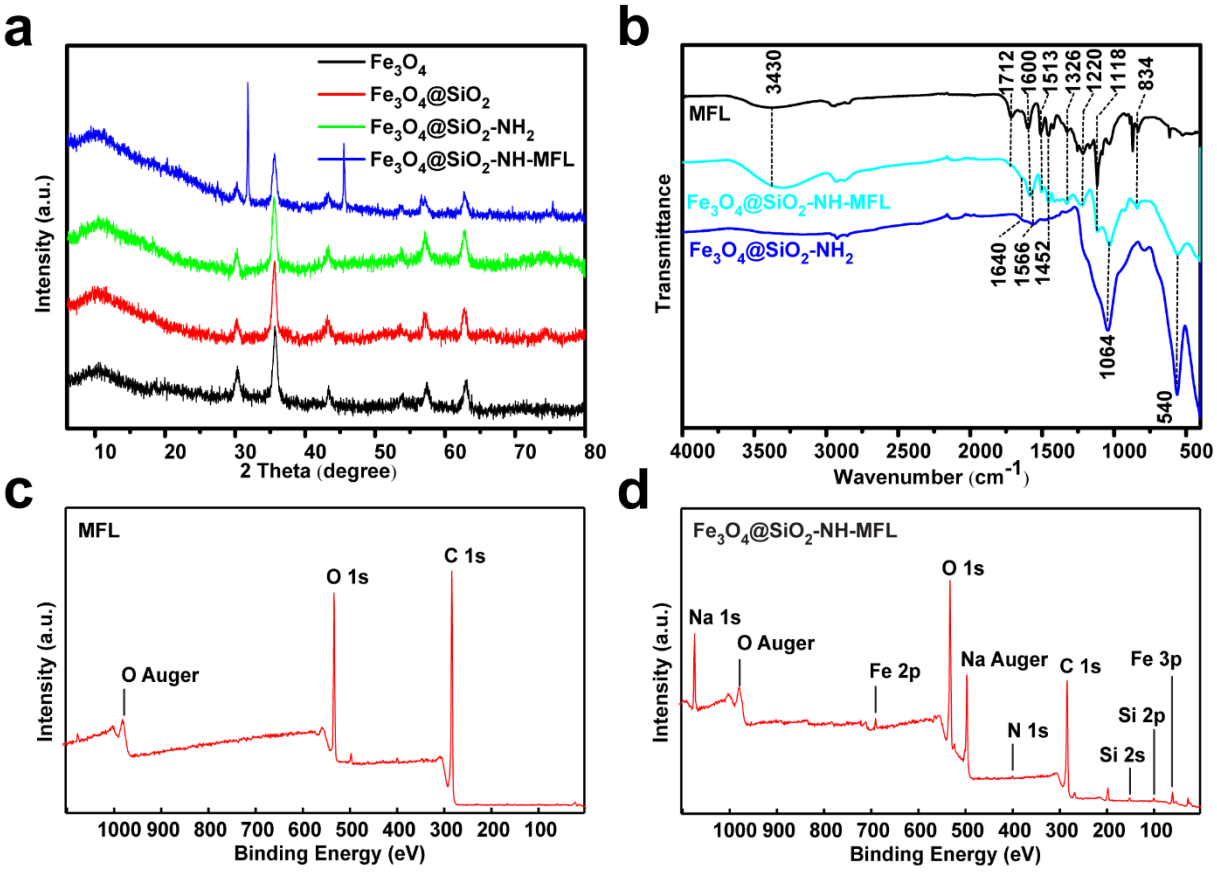

Fig. 2. Representative TEM images (left column) and SEM images (right column) of Fe_3O_4 (a and a_1), Fe_3O_4@SiO_2 (b and b_1), Fe_3O_4@SiO_2-NH_2 (c and c_1) and Fe_3O_4@SiO_2-NH-MFL (d and d_1).

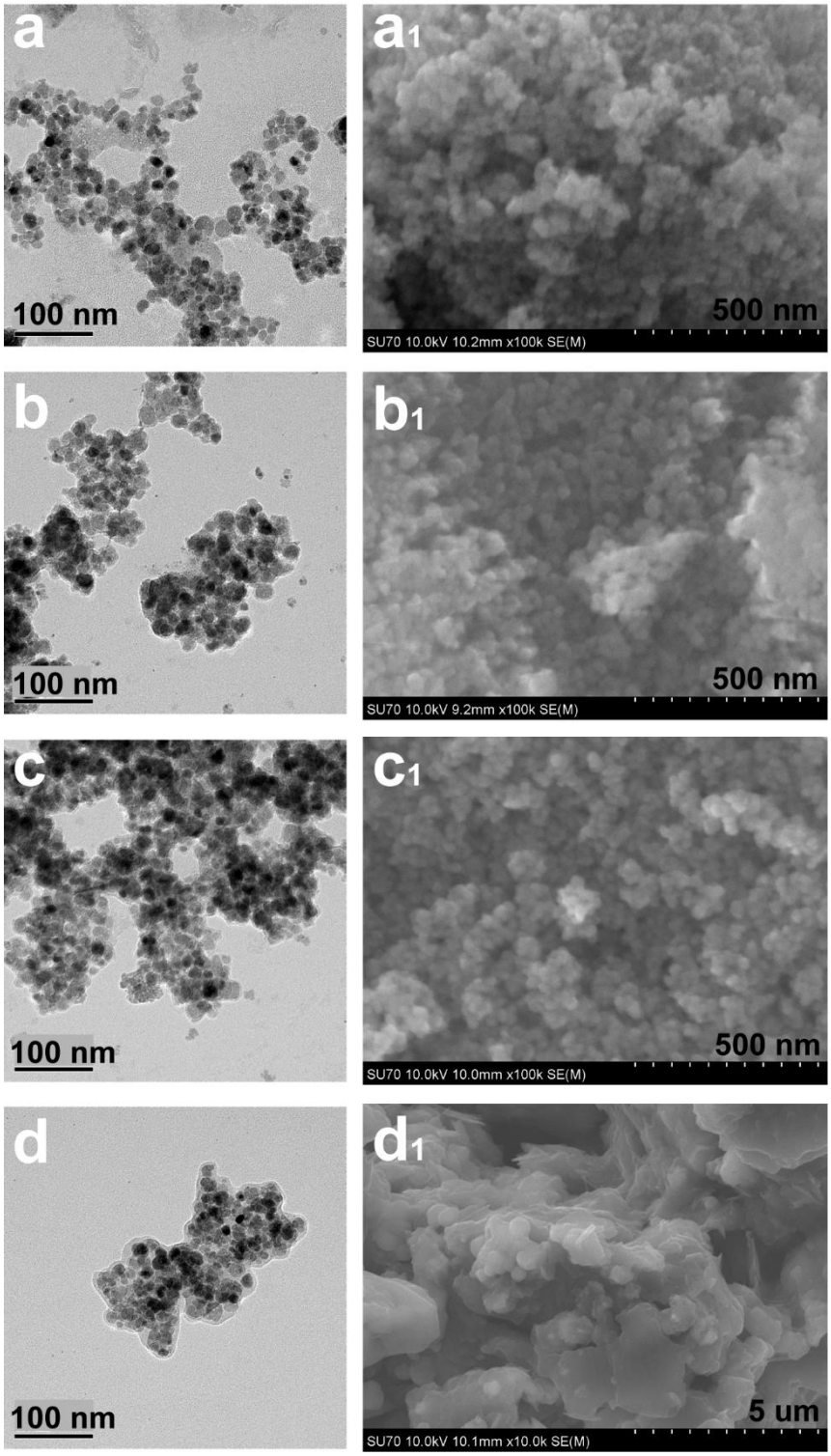

Fig. 3. (a) ζ-potentials of the synthesized nanoparticles as a function of pH. (b) The separation of Fe_3O_4@SiO_2-NH-MFL nanoparticles from suspension under an external magnetic field.

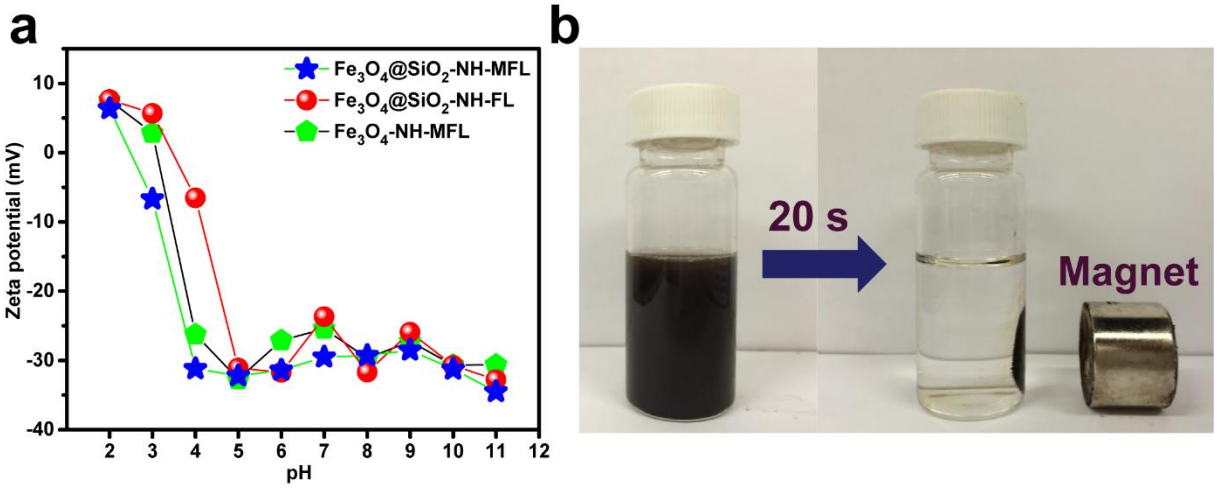

Fig. 4. (a) Effect of pH on the adsorption capacities of Pb^{2+} and (b) Cu^{2+} by Fe_3O_4@SiO_2-NH-MFL, Fe_3O_4@SiO_2-NH-FL and Fe_3O_4@SiO_2-MFL. (c) Effect of contact time on the adsorption capacity of Pb^{2+} and (d) Cu^{2+} by Fe_3O_4@SiO_2-NH-MFL. (e) Adsorption isotherms for Pb^{2+} and (f) Cu^{2+} adsorption on Fe_3O_4@SiO_2-NH-MFL and the corresponding Langmuir, Freundlich and Sips models

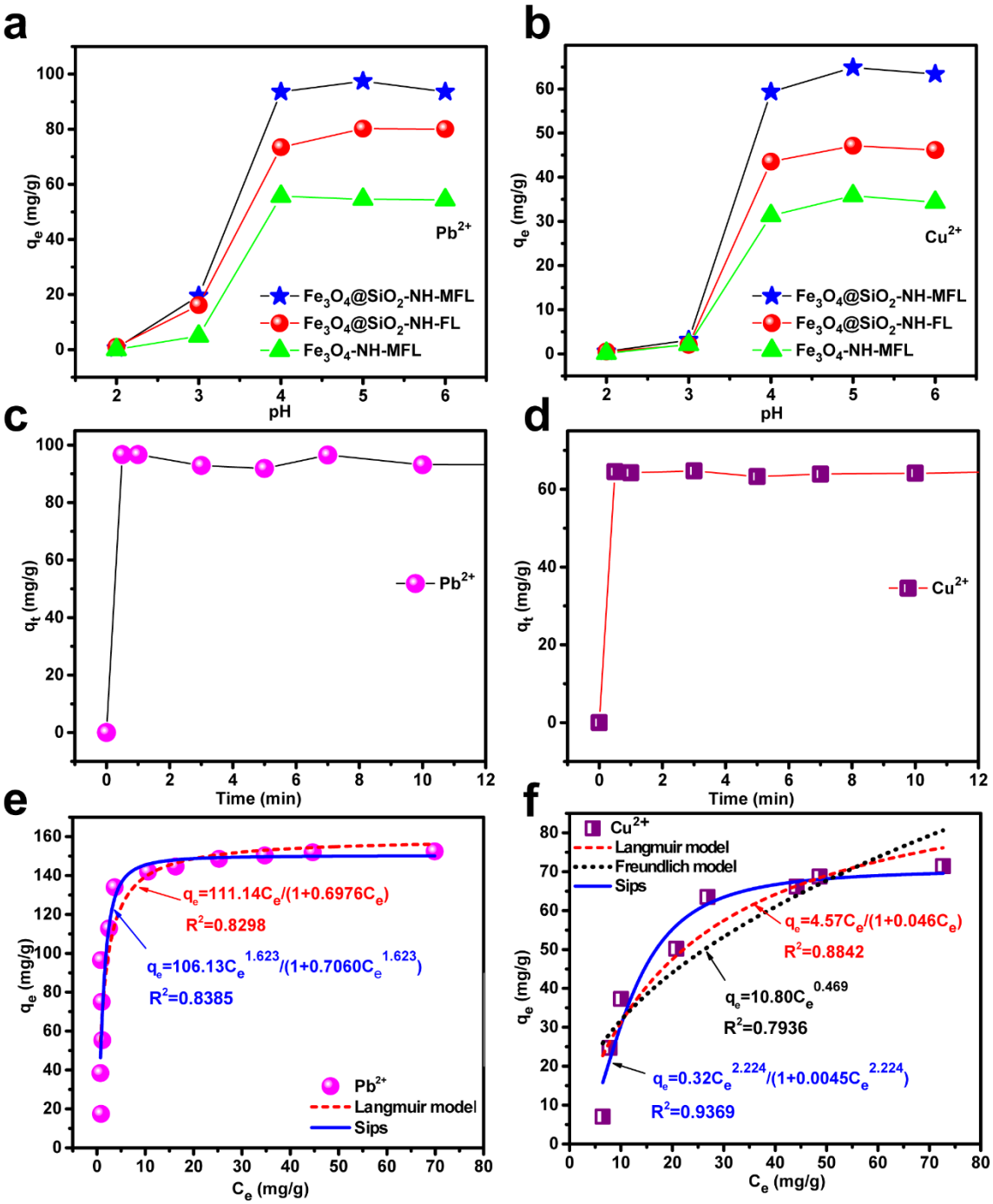

Fig. 5. FTIR analysis (a), XPS survey spectra (b), O 1s spectra (c and d) and C 1s spectra (e and f) of Fe_3O_4@SiO_2-NH-MFL before and after the adsorption of Pb^{2+} ions.